Michigan State University

National Superconducting Cyclotron Laboratory

NEW REGION OF DEFORMATION: THE NEUTRON-RICH SULFUR ISOTOPES

H. SCHEIT, T. GLASMACHER, B.A. BROWN, J.A. BROWN, P.D. COTTLE, P.G. HANSEN, R. HARKEWICZ, M. HELLSTRÖM, R.W. IBBOTSON, J.K. JEWELL, K.W. KEMPER, D.J. MORRISSEY, M. STEINER, P. THIROLF, and M. THOENNESSEN

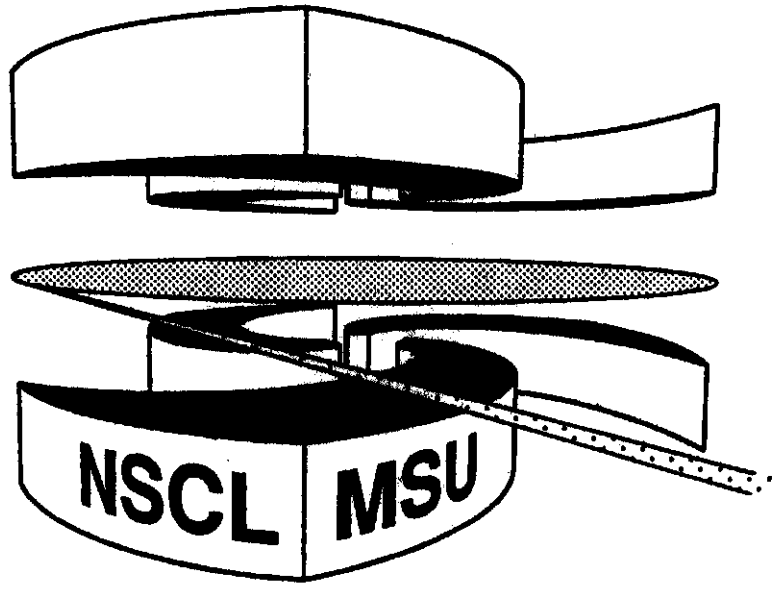

MSUCL-1029

AUGUST 1996

MSUCL-1029, to be published in Phys. Rev. Lett.

New region of deformation: the neutron-rich sulfur isotopes

H. Scheit[1,2], T. Glasmacher[1,2], B.A. Brown[1,2], J.A. Brown[1], P.D. Cottle[4], P.G. Hansen[1], R. Harkewicz[1], M. Hellström[5], R.W. Ibbotson[1], J.K. Jewell[4], K.W. Kemper[4], D.J. Morrissey[1,3], M. Steiner[1], P. Thirolf[1*], and M. Thoennessen[1,2]

[1] *National Superconducting Cyclotron Laboratory, Michigan State University, East Lansing, Michigan 48894*

[2] Department *of Physics and* Astronomy, *Michigan* State University, *East Lansing, Michigan 48824*

[3] *Department of Chemistry, Michigan State University, East Lansing, Michigan 48824*

[4] *Department of Physics, Florida State University, Tallahassee, Florida 32306*

[5] *Gesellschaft für Schwerionenforschung, D-64991 Darmstadt, Germany*

(September 11, 1996)

Abstract

The energies and $B(E2; 0^+_{g.s.} \rightarrow 2^+_1)$ values for the lowest $J^\pi = 2^+$ states in the neutron-rich radioactive nuclei ^{38,40,42}S and ^{44,46}Ar were measured via intermediate-energy Coulomb excitation. The results for ^{40,42}S provide the first evidence of moderate deformation near N = 28, while the effects of the N = 28 shell closure persist in the $Z = 18$ nucleus ^{46}Ar.

23.20.Lv, 25.70.De, 21.60.Cs, 27.30.+t, 27.40.+z

Typeset using REVTEX

*Current address: Ludwig Maximilians Universität München, D-85748 Garching, Germany.

One of the primary goals of experiments with radioactive beams is to determine how nuclear structure changes near the drip lines as the binding energies of single particle orbits approach zero. The region of β-unstable nuclei near the $N = 28$ isotope ^{44}S has attracted particular interest because these neutron-rich nuclei play an important role in the nucleosynthesis of the heavy Ca-Ti-Cr isotopes [1]. Werner *et al.* [2] suggested on the basis of self-consistent mean field calculations that the major $N = 28$ shell gap, which plays a defining role in the structure of $Z \geq 20$ nuclei, disappears at $Z = 16$, and they predicted moderate deformation for the neutron-rich sulfur isotopes. Radioactive beams are required to test these predictions because useful yields cannot be produced with fusion-evaporation or transfer reactions using stable beams and targets.

Here we report measurements of the energies and $B(E2; 0^+_{g.s.} \rightarrow 2^+_1)$ values for the 2^+_1 states of the neutron-rich isotopes ^{38,40,42}S and ^{44,46}Ar obtained with the technique of intermediate-energy Coulomb excitation [3] of beams of these radioactive nuclei. This technique has been used recently to populate low-lying states of several $A \leq 14$ nuclei [4] and ^{32}Mg [5]. The results reported here demonstrate, for the first time, that deformation occurs near $N = 28$ and that the $N = 28$ major shell gap persists in ^{46}Ar. Our data are compared to the results of calculations using two types of nuclear models. Werner *et al.* [2] calculated the properties of the nuclei measured here using self-consistent mean field techniques to account for the changes in binding energies and residual interactions that occur far from the line of stability. We also present shell model calculations that use empirical interactions obtained from nuclei closer to the beta-stability line and are, therefore, effectively an extrapolation from these nuclei.

The present experiment was performed at the National Superconducting Cyclotron Laboratory at Michigan State University. Primary beams of $^{48}Ca^{13+}$ and $^{40}Ar^{12+}$ with energies up to 80 MeV/nucleon and intensities as high as 5 pnA were produced with the NSCL room temperature electron cyclotron resonance (RTECR) ion source and the K1200 cyclotron. The ^{48}Ca beam was produced using a new technique discussed in [6]. The secondary sulfur and argon beams were obtained via the fragmentation of the primary beams in a 379 mg/cm^2

^{9}Be primary target located at the mid-acceptance target position of the A1200 fragment separator [7]. The rates and purities of the secondary beams are listed in Table I. The time of flight between a thin plastic scintillator located after the A1200 focal plane and a parallel plate avalanche counter (PPAC) located in front of the secondary target was recorded for each fragment and provided positive identification of the fragment before interaction in the target.

The position and direction of each fragment incident on the target (93.5 mg/cm^2 Au or 184.1 mg/cm^2 Au, see Table I) were measured with two PPACs. Fragments scattered into laboratory angles less than 4.1° were detected in a cylindrical fast plastic – slow plastic phoswich detector after passing through a third PPAC located in front of the phoswich detector. The energy loss – total energy measurements in the phoswich detector after the secondary target allowed us to reject events from the break-up of the projectile in the secondary target.

Photons were measured in coincidence with the scattered fragments in an array of 42 position sensitive NaI(Tl) detectors [8]. The NaI(Tl) crystals were cylindrical, 18 cm long, 5.75 cm in diameter and enclosed in a 0.45 mm thick aluminium shield and were oriented parallel to the beam direction, as shown in Fig. 1. The target was located perpendicular to the centerline of the detectors. The NaI(Tl) detectors were arranged around a 10.2 cm diameter aluminum beam pipe in three concentric rings. The energies and interaction points of the incident photons were reconstructed from photomultiplier tube signals at each end of the NaI(Tl) crystal. Photon sources of ^{22}Na, ^{88}Y, ^{152}Eu and ^{228}Th were used to obtain a position dependent energy calibration for each detector. The energy resolution of the detectors was typically 8% at 662 keV. The position resolution was approximately 2 cm. This resulted in an angular resolution of better than 10° for the emitted photon. The angular information was used to correct for the large Doppler shift of the photons emitted from the secondary beam particles. To shield the NaI(Tl) detector array from photons originating at the zero degree phoswich detector, the PPACs, and from room background, the entire array was surrounded by a 16.6 cm thick layer of low-background lead bricks.

The time difference between the detection of the photon in the NaI(Tl) detectors and the detection of the scattered fragment in the zero degree detector was recorded for each event so that accidental coincidences could be subtracted from the γ-ray spectra. Coincident photons in ^{22}Na and ^{88}Y as well as a ^{152}Eu source were used to measure the energy- and position-dependent photo-peak efficiency of the NaI(Tl)-array. The detector efficiency was folded with the photon angular distribution [9] in the projectile frame to determine the photopeak detection efficiency for a photon emitted from the excited projectile. This was combined with the integrated number of beam particles as identified in the zero-degree detector ($\theta_{\rm lab} \leq 4.1°$) and the target thickness to obtain the cross sections in Table I. From these cross sections we then determined $B(E2; 0^+_{g.s.} \rightarrow 2^+_1)$ and β_2 [11] values assuming pure intermediate energy Coulomb excitation [3]. Neglecting nuclear excitation is justified here as a typical distance of closest approach between the projectile and the target in this experiment is 18 fm, which is about 5 fm more than the distance between projectile and target assuming touching spheres. We also used the coupled channels code ECIS [13] to verify that the nuclear contribution to the cross sections in the angular range covered by the zero degree detector is negligible. These calculations used standard collective model form factors and the optical model potential given by Suomijärvi *et al.* for the ^{40}Ar+^{208}Pb reaction at 41 MeV/nucleon [14].

Photons emitted from the fast moving fragments ($v \approx 0.3c$) could be clearly distinguished from photons emitted from the stationary target by their Doppler shifts. Figure 2 shows the γ-ray energy spectrum as a function of position in the NaI(Tl) detectors for the ^{40}S+^{197}Au reaction. The left panel shows the γ-ray energies in the laboratory rest frame; that is, before any Doppler shift adjustment. In this panel, the energy of the 547 keV ($\frac{7}{2}^+ \rightarrow g.s.$) transition from the ^{197}Au target is independent of position, while the energy observed for the $2^+_1 \rightarrow 0^+_{g.s.}$ γ-ray from the projectile ^{40}S depends strongly on the position and, therefore, on the angle at which it was emitted. The right panel shows the same energy spectrum with a Doppler shift to the projectile rest frame ($v = 0.27c$, corresponding to the velocity of the projectile at the mid point of the target). In this panel, the energy of the γ-ray from

the projectile is constant, while the energy of the target γ-ray now varies as a function of position. Similar comparisons were used to distinguish between target and projectile γ-rays for all the nuclei studied here.

The Doppler-corrected, background-subtracted γ-ray spectra for all five nuclei studied here are shown in Fig. 3. All five spectra clearly show one photopeak associated with each projectile. To address the question of whether the observed γ-rays might be produced by 3^- states instead of 2^+ states, coupled channels calculations were performed with the computer code ECIS88 [13] as described above. The calculated cross sections for populating 2^+ states were at least a factor of five larger than the 3^- cross sections if one assumes identical excitation energies and coupling strengths for the two states. We therefore conclude that the observed γ-rays correspond to the $2_1^+ \rightarrow 0_{g.s.}^+$ transitions in the projectiles. The measured energies of the 2_1^+ states and $B(E2; 0_{g.s.}^+ \rightarrow 2_1^+)$ values are listed in Table I. It should be noted that the $B(E2; 0_{g.s.}^+ \rightarrow 2_1^+)$ result obtained here for ^{38}S is consistent with the lower limit set on the lifetime of the 2_1^+ state by Olness *et al.* [15]. In addition, the well-known energy of the 2_1^+ state of ^{38}S [16] was used to check the energy calibration procedure.

No excited states have been observed previously in ^{40,42}S, but excited states have been reported for ^{44,46}Ar [17,18]. Crawley *et al.* [17] observed states in ^{44}Ar using the ^{48}Ca(^{3}He,^{7}Be) reaction and proposed the 2_1^+ state of ^{44}Ar to be at 1.61 MeV. The spectra in the study of Crawley *et al.* are quite difficult to interpret because the background peaks are much larger than those from ^{44}Ar. If the 1.144 MeV state proposed here as the 2_1^+ state was populated in the experiment of Crawley *et al.*, it would have been obscured by a peak corresponding to an excited state of ^{7}Be. Mayer *et al.* [18] reported an energy of 1.55 MeV for the corresponding state in ^{46}Ar from their work with the ^{48}Ca(^{14}C,^{16}O) reaction in agreement with the present work.

Self-consistent mean field techniques [2] predict permanent quadrupole deformations in ^{40,42}S of $\beta_2 \sim 0.25$, only slightly smaller than those measured here (see Table I). However, in these calculations prolate and oblate predictions are practically degenerate. Our data do not allow us to distinguish between these two shapes, either. For ^{44,46}Ar, Werner *et*

al. [2] did not provide definitive predictions, but instead showed that their two calculation techniques (Hartree-Fock+Skyrme and relativistic mean field) give very different answers for these two nuclei. The Hartree-Fock calculations yield a significant prolate deformation ($\beta_2 = +0.17$) for ^{44}Ar and an oblate deformation ($\beta_2 = -0.13$) for ^{46}Ar. On the other hand, the relativistic mean field calculations yield $\beta_2 = -0.13$ for ^{44}Ar and $\beta_2 = 0.00$ for ^{46}Ar. The experimental $B(E2; 0^+_{g.s.} \rightarrow 2^+_1)$ results agree with the Hartree-Fock results better, since we measure a non-zero deformation for ^{46}Ar ($\beta_2 = 0.18(2)$) and a relatively large deformation for ^{44}Ar ($\beta_2 = 0.24(2)$), though we are unable to determine the *signs* of the deformations. The effects of the $N = 28$ major shell gap persist in ^{46}Ar because it is less deformed than ^{44}Ar and its deformation and the energy of its first excited state are similar to ^{50}Ti (E(2^+_1) = 1554 keV, $\beta_2 = 0.17$, [19]). It would be of considerable interest to measure the 2^+_1 state of ^{44}S to see whether the $N = 28$ shell gap is still present even further from the line of stability.

While the shapes of ^{40,42}S can be understood with the mean field calculations of Werner *et al.* [2] which attempt to account for changes in single particle binding energies and residual interactions away from the line of stability, the data for all nuclei measured here except ^{46}Ar can also be explained with shell model calculations which use empirical interactions obtained from nuclei close to the stability line. These calculations were carried out in a model space in which the protons occupy the $0d_{5/2}$, $0d_{3/2}$ and $1s_{1/2}$ (sd) orbitals and the neutrons occupy the $0f_{7/2}$, $1p_{3/2}$, $0f_{5/2}$ and $1p_{1/2}$ (pf) orbitals. For many of the nuclei under consideration the dimension of the full $\pi(sd)$-$\nu(pf)$ model space is too large, and the calculations reported here have been truncated by leaving out the $0f_{5/2}$ and $1p_{1/2}$ neutron orbitals. With this truncation the dimension for the 2^+ state in ^{42}S is 4335. For some nuclei such as ^{48}Ca and ^{46}Ar, this truncation can be compared to those performed in a model space which includes the $0f_{5/2}$ and $1p_{1/2}$ orbitals, and the results for the orbital occupations and excitation energies of the 2^+ states are found to be very similar. We use the Wildenthal sd-shell interaction [20], the recent FPD6 pf-shell interaction [21] and the WBMB $sd - pf$ cross-shell interaction [22]. This latter cross-shell interaction successfully accounts for the properties of the $N = 20 - 22$ nuclei including the intruder state deformation in ^{32}Mg [22].

The B(E2) values were calculated using proton and neutron effective charges of $e_p = 1.6e$ and $e_n = 0.9e$, respectively, which were chosen to reproduce the E2 transition strengths of the proton *sd*-shell transitions in ^{36}S and ^{38}Ar [16] and neutron *pf*-shell transitions in ^{48}Ca [23].

In the top two panels of Fig. 4, the measured β_2 values are compared to the results of the mean field calculations of Werner *et al.* and the present shell model calculations. The mean field calculations slightly underpredict the measured values for ^{40,42}S and the shell model calculations slightly overpredict β_2 for these nuclei. However, the shell model calculation predicts that the β_2 value in ^{46}Ar is *larger* than in ^{44}Ar, contrary to the downward trend in the data, which can be explained by the persistence of the $N = 28$ shell closure. The increase in $B(E2)$ for the shell-model calculation is related to the crossing of the $0d_{3/2}$ and $1s_{1/2}$ proton orbitals observed between ^{35}K (which has a $3/2^+$ ground state [16]) and ^{37}K (which has a $1/2^+$ ground state [16]). The bottom two panels of Fig. 4 show that the shell model calculations successfully reproduce the behavior of $E(2_1^+)$ in the nuclei reported here.

The results presented here demonstrate that a direct measurement of $B(E2; 0_{g.s.}^+ \rightarrow 2_1^+)$ is necessary to determine the nuclear deformation, and that the energies of the 2_1^+ states (without the $B(E2)$ values) are not sufficient to deduce the deformation on the basis of systematics. For example, the global systematics of Raman *et al.* [12] give $\beta_2 = 0.4$ from the energies of the 2_1^+ states in ^{40,42}S. The experimental β_2 deformations are significantly smaller.

In summary, the energies and $B(E2; 0_{g.s.}^+ \rightarrow 2_1^+)$ values of the 2_1^+ states of ^{38,40,42}S and ^{44,46}Ar have been measured using intermediate-energy Coulomb excitation. The isotopes ^{40,42}S are deformed, indicating the presence of a new region of deformed nuclei near $N = 28$. The data on the 2_1^+ state in ^{46}Ar demonstrate that the $N = 28$ major shell gap persists at $Z = 18$. Both the mean field calculations and shell model calculations using empirical interactions can approximately reproduce the behavior of the 2_1^+ states of ^{40,42}S. A measurement of ^{44}S will show whether the $N = 28$ shell gap, which is still evident in ^{46}Ar, persists to $Z = 16$.

We thank Professor Lee Sobotka (Washington University) for making the detectors avail-

able to us, the NSCL operations group for providing the ^{48}Ca beam and Dr. N. Alamanos for assistance with the ECIS calculations. M. H. acknowledges the support of the Alexander von-Humboldt Foundation. This work was supported by the National Science Foundation under Grant Nos. PHY-9528844, PHY-9523974 and PHY-9403666.

REFERENCES

[1] O. Sorlin *et al.*, Phys. Rev. C **47**, 2941 (1993).

[2] T.R. Werner *et al.*, Phys. Lett. B **335**, 259 (1994); Nucl. Phys. A **597**, 327 (1996).

[3] A. Winther and K. Alder, Nucl. Phys. A **319**, 518 (1979).

[4] R. Anne *et al.*, Z. Phys. A **352**, 397 (1995).

[5] T. Motobayashi *et al.*, Phys. Lett. B **346**, 9 (1995).

[6] R. Harkewicz, Rev. Sci. Instr. **67**, 2176-2178 (1996).

[7] B.M. Sherrill *et al.*, Nucl. Instr. Methods **B56**, 1106 (1991).

[8] T. Glasmacher, P. Thirolf, and H. Scheit (to be published).

[9] The angular distributions of the photons (in particular the population of the magnetic substates in the 2^+ state) were calculated using Winther and Alder's theory of relativistic Coulomb excitation [3] combined with their work on photon angular distributions [10].

[10] K. Alder *et al.*, Rev. Mod. Phys. **28**, 432 (1956).

[11] We use $\beta_2 = \frac{4\pi}{3ZR_0^2}(B(E2\uparrow))^{1/2}$ with $R_0 = 1.2A^{1/3}$fm and $B(E2)$ in units of e^2fm^4 [12].

[12] S. Raman *et al.*, Phys. Rev. C **43**, 556 (1991).

[13] J. Raynal, Computer code ECIS88, unpublished.

[14] T. Suomijärvi *et al.*, Nucl. Phys. A **509**, 369 (1990).

[15] J.W. Olness *et al.*, Phys. Rev. C **34**, 2049 (1986).

[16] P.M. Endt, Nucl. Phys. A **521**, 1 (1990).

[17] G.M. Crawley *et al.*, Phys. Lett. B **64**, 143 (1976).

[18] W. Mayer *et al.*, Phys. Rev. C **22**, 2449 (1980).

[19] S. Raman *et al.*, At. Data Nucl. Data Tables **36**, 1 (1987).

[20] B.A. Brown and B.H. Wildenthal, Ann. Rev. Nucl. Sci. **38**, 29 (1988).

[21] W.A. Richter *et al.*, Nucl. Phys. **A523**, 325 (1991).

[22] E.K. Warburton, J.A. Becker and B.A. Brown, Phys. Rev. C**41**, 1147 (1990).

[23] G. Krause *et al.*, Phys. Rev. Lett. 73, 1773 (1994).

FIGURES

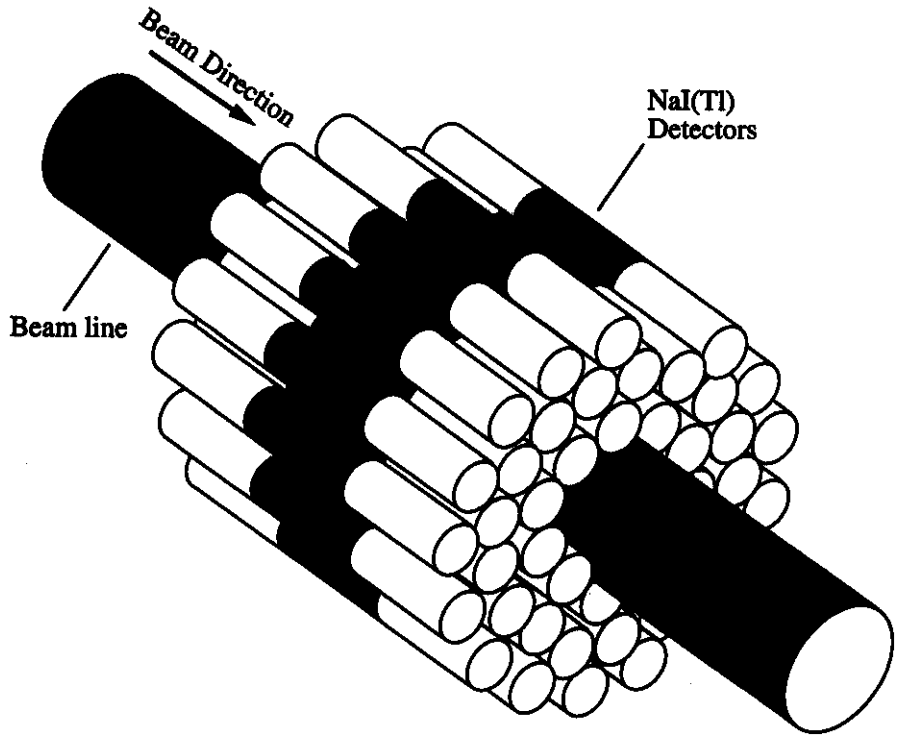

FIG. 1. Arrangement of the position sensitive NaI(Tl) detectors in the experiment.

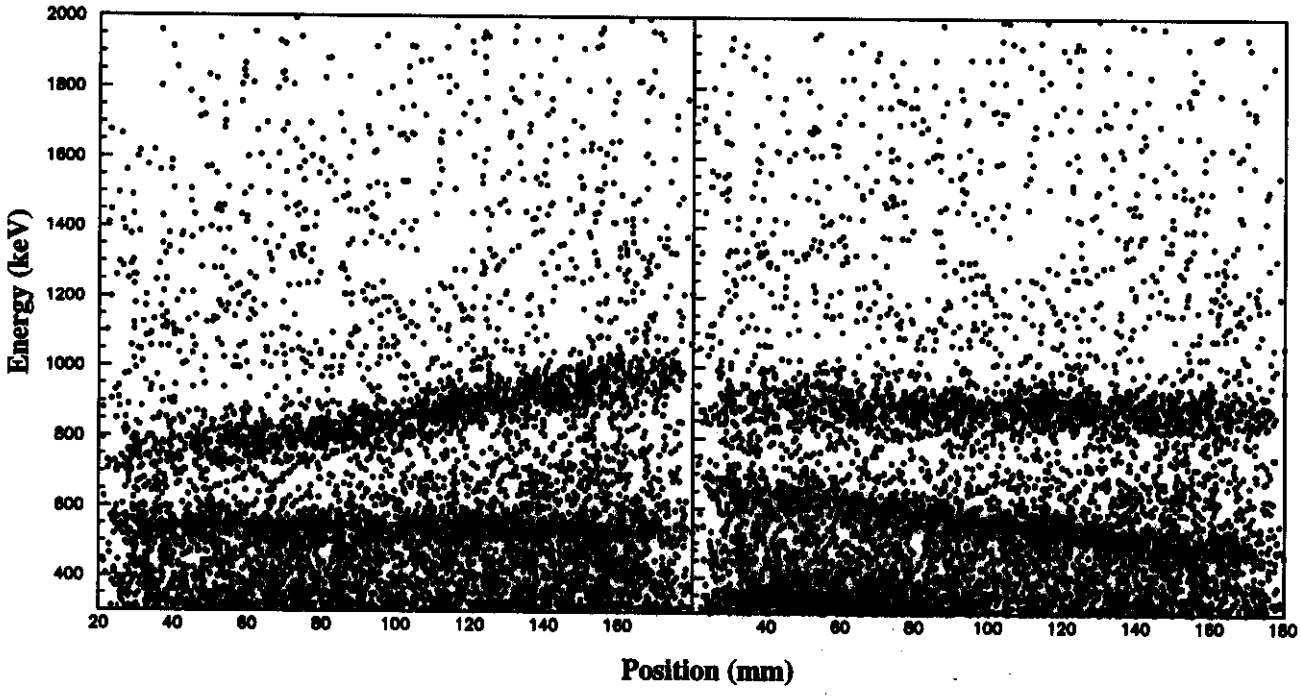

FIG. 2. Observed energies of γ-rays as a function of position without correction for Doppler shifting (left panel) and with the Doppler correction (right panel) for the ^{40}S+^{197}Au reaction. The target was located in the middle. The γ-rays near 547 keV are from the gold target, while those near 890 keV are from the $2_1^+ \rightarrow 0_{g.s.}^+$ transition in the projectile, as discussed in the text.

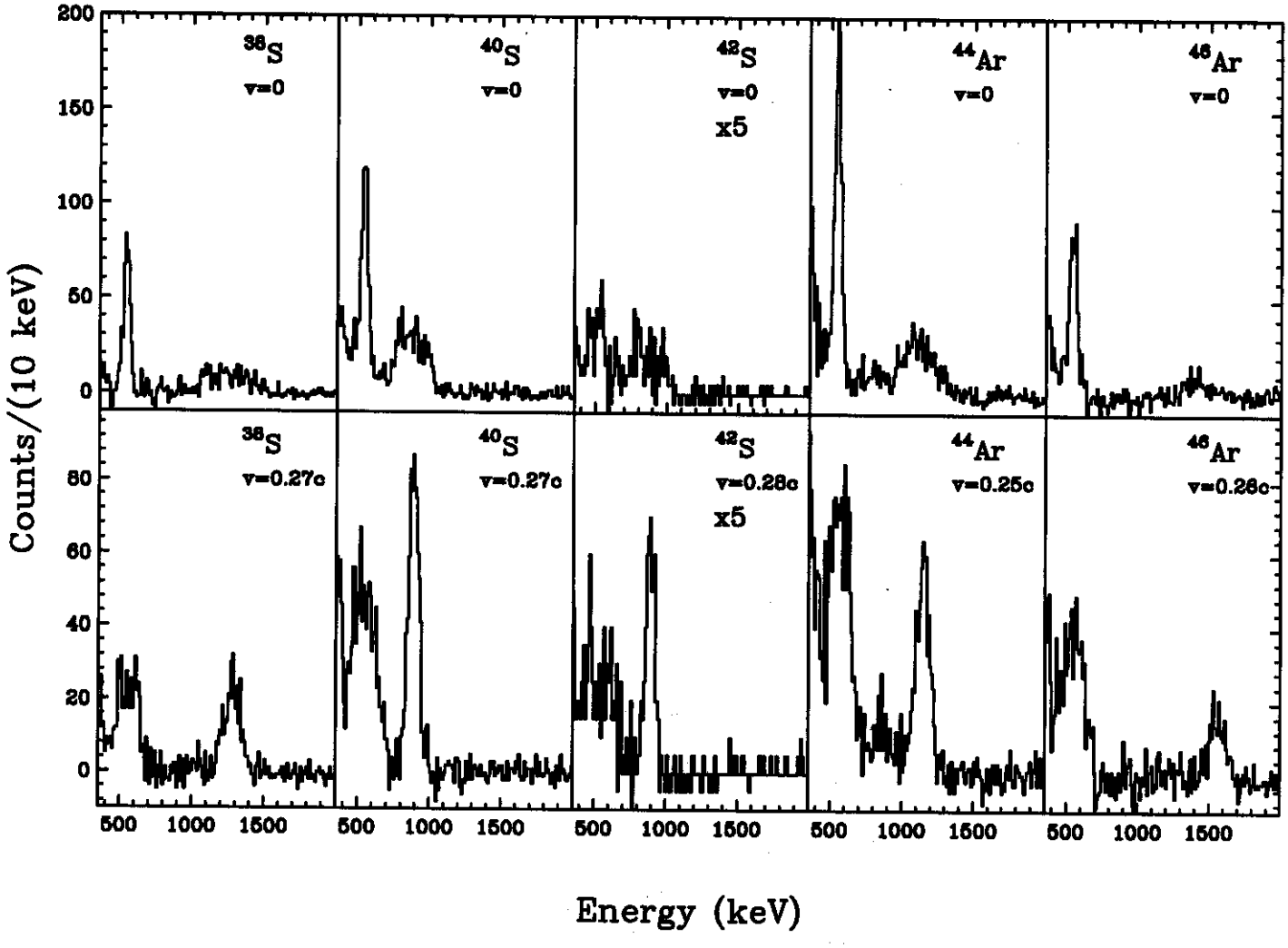

FIG. 3. Upper panels contain background subtracted photon spectra in the laboratory frame. The 547 keV ($7/2^+ \rightarrow g.s.$) transition in the gold target is visible as a peak, while the ($2^+ \rightarrow g.s.$) transitions in each projectile are very broad. Lower panels contain Doppler-corrected, background-subtracted γ-ray spectra.

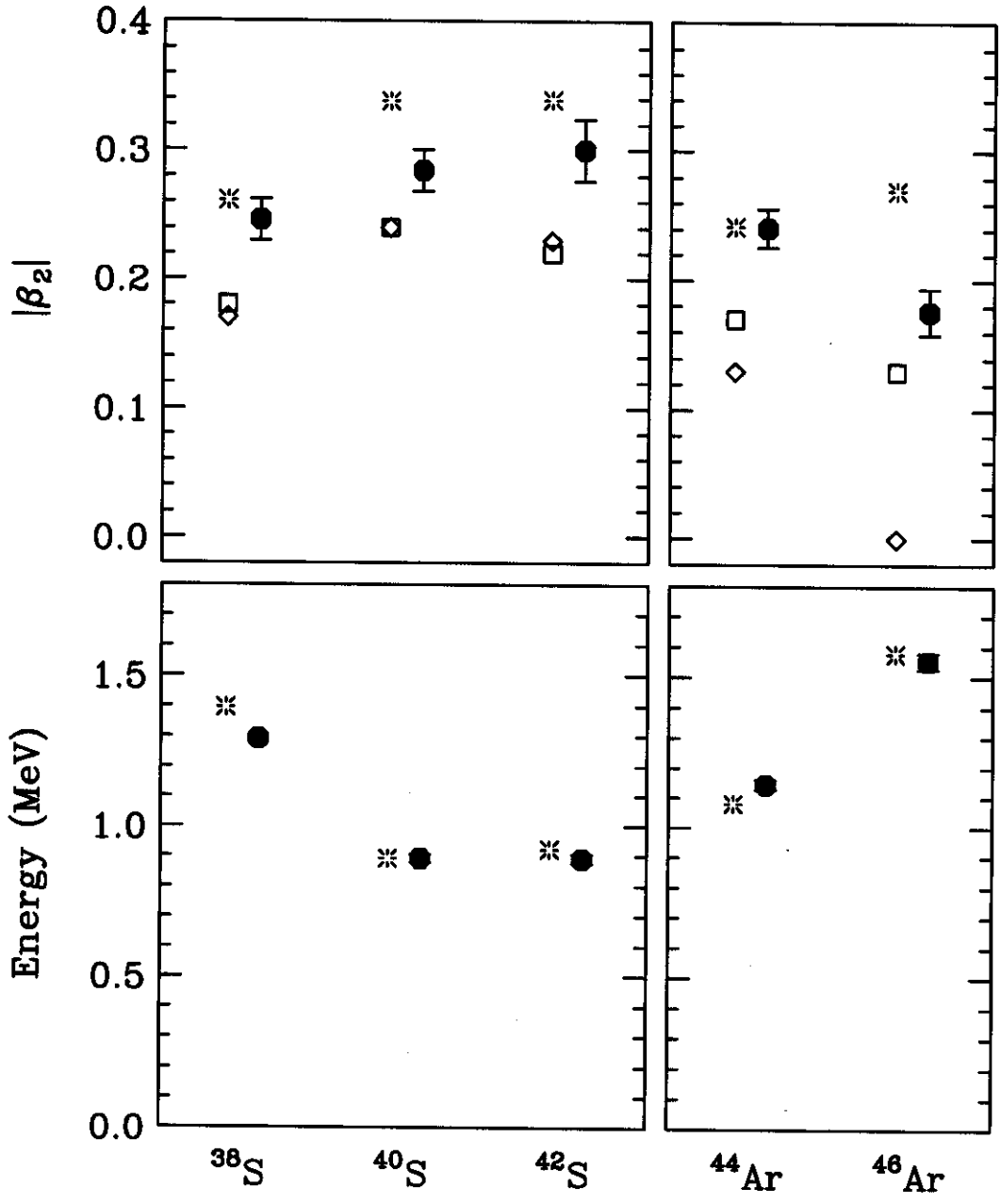

FIG. 4. The top two panels compare the experimental quadrupole deformation parameters $|\beta_2|$ [11] (solid points) to shell model calculations (stars) described in the text and to relativistic mean field (open diamonds) and Hartree-Fock (open squares) predictions [2]. The bottom two panels show a comparison between the experimentally observed excitation energies $E(2^+)$ (solid points) of the first excited states and the shell model calculations (stars) described in the text.

TABLES

TABLE I. Experimental parameters and results. The purity of the secondary beam is for reference only; the secondary fragments were positively identified on an event by event basis and only desired fragments were analyzed. The relationship between $B(E2;0^+_{g.s.} \rightarrow 2^+_1))$ and β_2 is given in [11].

secondary beam	^{38}S	^{40}S	^{42}S	^{44}Ar	^{46}Ar
Energy (MeV/nucleon)	39.2	39.5	40.6	33.5	35.2
Energy spread	±3%	±3%	±3%	±3%	±3%
Beam purity	0.99	0.65	0.55	0.99	0.99
typ. intensity on target (s^{-1})	50,000	17,000	1,800	50,000	27,000
secondary Au target (mg/cm^2)	184.1	184.1	184.1	93.5	93.5
Energy loss in target (MeV/nucleon)	9.1	8.4	7.9	5.1	4.9
Energy of first excited state (keV)	1286(19)	891(13)	890(15)	1144(17)	1554(26)
$\sigma(E2; 0^+_{g.s.} \rightarrow 2^+_1, \theta_{lab} \leq 4.1°)$(mbarn)	59(7)	94(9)	128(19)	81(9)	53(10)
$B(E2;0^+_{g.s.} \rightarrow 2^+_1))$ (e^2fm^4)	235(30)	334(36)	397(63)	345(41)	196(39)
$\lvert\beta_2\rvert$	0.246(16)	0.284(16)	0.300(24)	0.241(14)	0.176(17)